Article

Neuron

Memory-Relevant Mushroom Body Output Synapses Are Cholinergic

Highlights

- Mushroom body Kenyon cell function requires ChAT and VAChT expression
- Kenyon cell-released acetylcholine drives mushroom body output neurons
- Blocking nicotinic receptors impairs mushroom body output neuron activation
- Acetylcholine interacts with coreleased neuropeptide

Authors

Oliver Barnstedt, David Owald, Johannes Felsenberg, ..., Clifford B. Talbot, Paola N. Perrat, Scott Waddell

Correspondence

david.owald@charite.de (D.O.), scott.waddell@cncb.ox.ac.uk (S.W.)

In Brief

Fruit fly memory involves plasticity of mushroom body synapses. Barnstedt et al. identified acetylcholine as the mushroom body neurotransmitter. Mushroom body output neuron activation requires nicotinic acetylcholine receptors. Impaired receptor function reduces physiological responses and alters odor-driven behavior.

Barnstedt et al., 2016, Neuron *89*, 1237–1247
March 16, 2016
http://dx.doi.org/10.1016/j.neuron.2016.02.015

CellPress

Neuron
Article

Memory-Relevant Mushroom Body Output Synapses Are Cholinergic

Oliver Barnstedt,[1] David Owald,[1,3,*] Johannes Felsenberg,[1] Ruth Brain,[1] John-Paul Moszynski,[1] Clifford B. Talbot,[1] Paola N. Perrat,[2] and Scott Waddell[1,*]
[1]Centre for Neural Circuits and Behaviour, The University of Oxford, Tinsley Building, Mansfield Road, Oxford OX1 3SR, UK
[2]Department of Neurobiology, UMass Medical School, Worcester, MA 01605, USA
[3]Present address: Institute of Neurophysiology, Charité – Universitätsmedizin Berlin, 10117 Berlin, Germany
*Correspondence: david.owald@charite.de (D.O.), scott.waddell@cncb.ox.ac.uk (S.W.)
http://dx.doi.org/10.1016/j.neuron.2016.02.015

SUMMARY

Memories are stored in the fan-out fan-in neural architectures of the mammalian cerebellum and hippocampus and the insect mushroom bodies. However, whereas key plasticity occurs at glutamatergic synapses in mammals, the neurochemistry of the memory-storing mushroom body Kenyon cell output synapses is unknown. Here we demonstrate a role for acetylcholine (ACh) in *Drosophila*. Kenyon cells express the ACh-processing proteins ChAT and VAChT, and reducing their expression impairs learned olfactory-driven behavior. Local ACh application, or direct Kenyon cell activation, evokes activity in mushroom body output neurons (MBONs). MBON activation depends on VAChT expression in Kenyon cells and is blocked by ACh receptor antagonism. Furthermore, reducing nicotinic ACh receptor subunit expression in MBONs compromises odor-evoked activation and redirects odor-driven behavior. Lastly, peptidergic corelease enhances ACh-evoked responses in MBONs, suggesting an interaction between the fast- and slow-acting transmitters. Therefore, olfactory memories in *Drosophila* are likely stored as plasticity of cholinergic synapses.

INTRODUCTION

Understanding how memories are formed, stored, and retrieved from neural networks is an important pursuit of neuroscience. The insect mushroom bodies (MBs) are prominent bilateral brain structures that have been extensively studied for their universal role in learned behavior (Strausfeld et al., 1998; Heisenberg, 2003; Farris, 2013; Perisse et al., 2013a; Menzel, 2014). In the larger eusocial insects, such as honeybees, the MBs are comprised of a few 100,000 intrinsic neurons or Kenyon cells (KCs), whereas the smaller fruit fly MBs have only around 2,000 neurons per hemisphere. The anatomy of the MB has been compared to the fan-out, fan-in neural architecture of the mammalian cerebellum and hippocampus (Farris, 2011; Stevens, 2015; Menzel, 2014; Owald and Waddell, 2015) and to the cephalopod vertical lobes (Shomrat et al., 2011). Analogies have also been drawn to the vertebrate amygdala, basal ganglia, and pallium (Hige et al., 2015; Waddell 2013; Tomer et al., 2010). It is therefore of interest to understand the logic of how the MB operates and to what level functional principles relate to those of similar neural structures across phyla. Importantly, recent studies suggest that in the *Drosophila* MB cellular mechanisms of neural plasticity can be directly linked to behavioral change (Owald et al., 2015).

In all insects the axons from different subpopulations of KCs are arranged into separate parallel bundles, or lobes (Strausfeld et al., 2009). Some of the anatomical subdivision serves individual sensory modalities such as olfaction, gustation, and vision (Strausfeld et al., 1998; Murthy et al., 2008; Honegger et al., 2011; Campbell et al., 2013; Caron et al., 2013; Vogt et al., 2014; Aso et al., 2014a), while certain KCs may be multimodal (Strausfeld et al., 2009; Kirkhart and Scott, 2015). The primary sensory input to *Drosophila* KCs occurs in the MB calyx where their dendrites receive divergent fan-out input from around 50 classes of cholinergic olfactory projection neurons (Yasuyama et al., 2002; Caron et al., 2013). Odor-specific activity in the projection neuron population is transformed into activation of fairly sparse subpopulations of KCs across the $\alpha\beta$, $\alpha'\beta'$ and γ divisions in the overall MB ensemble (Honegger et al., 2011; Campbell et al., 2013; Lin et al., 2014a). Reinforcing dopaminergic neurons that innervate nonoverlapping zones of the MB lobes are believed to assign positive or negative values to odor-activated KCs during learning (Mao and Davis, 2009; Claridge-Chang et al., 2009; Aso et al., 2012; Liu et al., 2012; Burke et al., 2012; Waddell, 2013). Comprehensive anatomical studies have characterized all of the dopaminergic input and the output pathways of the MB (Tanaka et al., 2008; Aso et al., 2014a). Remarkably, information from the 2,000 KCs converges, or fans-in, onto the dendrites of 21 different types of mushroom body output neurons (MBONs). The MBONs tile the MB lobes into 15 discrete compartments, and each one has a corresponding set of afferent dopaminergic neurons (DANs). This anatomy alone suggests that learning-related plasticity alters odor drive to downstream MBONs whose dendrites occupy the same zones as the reinforcing dopaminergic neurons (Aso et al., 2014b; Owald and Waddell, 2015). Indeed, several studies have shown that reinforcer quality is represented in discrete dopaminergic zones on the MB lobes (Aso et al., 2012; Das et al., 2014; Galili et al., 2014; Lin et al., 2014b; Huetteroth et al., 2015; Yamagata et al., 2015) and have documented altered odor drive to specific MBONs after learning (Séjourné et al., 2011; Plaçais et al.,

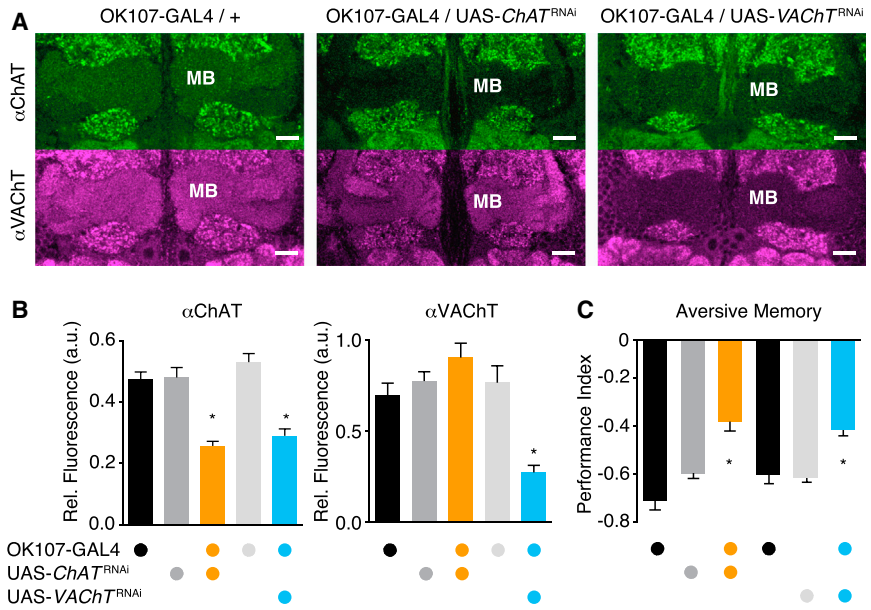

Figure 1. Kenyon Cells Express ChAT and VAChT, and Compromised *ChAT* or *VAChT* Expression Impairs MB Function

(A) MBs label with an antibody to ChAT (upper row) and an antibody to VAChT (bottom row). Pseudocolored images of single confocal sections at the level of the MB γ lobe. OK107-GAL4-driven UAS-*ChAT*^{RNAi} in KCs reduces anti-ChAT label in the MB. UAS-*VAChT*^{RNAi} reduces anti-ChAT and anti-VAChT immunoreactivity in MB. See Figure S1 for additional data. Scale bar, 20 μm.

(B) Quantification of (A). Anti-ChAT label is significantly lower in MBs in UAS-*ChAT*^{RNAi};OK107-GAL4 and UAS-*VAChT*^{RNAi};OK107-GAL4 flies as compared to all genetic controls. Anti-VAChT signal is significantly lower in MBs in UAS-*VAChT*^{RNAi};OK107-GAL4 flies (n = 3–9, asterisks denote $p < 0.05$; one-way ANOVA, Tukey's HSD post hoc test). Similar results are evident in the α, α′, β, and β′ lobes (data not shown).

(C) Aversive olfactory memory expression requires ACh function in KCs. Performance of UAS-*ChAT*^{RNAi};OK107-GAL4 and UAS-*VAChT*^{RNAi};OK107-GAL4 flies is significantly different from that of heterozygous controls (n = 6, asterisks denote $p < 0.01$; one-way ANOVA, Tukey's HSD post hoc test). See Figures S2A–S2C for additional experiments. Error bars in (B) and (C) represent the standard error of the mean (SEM).

2013; Pai et al., 2013; Owald et al., 2015; Bouzaiane et al., 2015). Interestingly, reward learning appears to reduce drive to output pathways that direct avoidance behavior, whereas aversive learning increases drive to avoidance pathways while reducing drive to approach pathways (Owald et al., 2015). Learning requires dopamine receptors and cAMP signaling in the KCs (Kim et al., 2007; Qin et al., 2012; Zars et al., 2000; McGuire et al., 2003; Blum et al., 2009; Trannoy et al., 2011), which implies a presynaptic mechanism of plasticity at KC-MBON junctions. In fact, a recent study (Hige et al., 2015) demonstrated that pairing odor presentation with activation of aversive dopaminergic neurons drives odor-specific synaptic depression at KC-MBON junctions. Despite considerable progress in understanding how memory is coded in the MB network, the fast-acting neurotransmitter of the underlying KC-MBON synapses that are modified by learning is not known.

Classic examples of plasticity in *Aplysia* and mammals involve presynaptic and/or postsynaptic effects at glutamatergic synapses (Roberts and Glanzman, 2003; Kandel et al., 2014). Although a small number of *Drosophila* KCs can be labeled with antibodies to glutamate, aspartate, or taurine (Schäfer et al., 1988; Schürmann, 2000; Sinakevitch et al., 2001; Strausfeld et al., 2003), immunostaining cannot differentiate between these molecules being transmitters or simply metabolites. Moreover, expression of the vesicular glutamate transporter is prominent in the fly brain but notably absent from the MB (Daniels et al., 2008). Immunohistochemical studies also suggested that, unlike much of the fly brain, KCs do not express the acetylcholine (ACh) synthesizing enzyme choline acetyltransferase (ChAT) (Gorczyca and Hall, 1987; Buchner et al., 1986; Yasuyama et al., 1995b).

Here we demonstrate using neurochemical, physiological, and behavioral approaches that ACh is a neurotransmitter of the *Drosophila* KCs. A significant part of KC-MBON communication is carried by cholinergic transmission from KCs that activates nicotinic ACh receptors on MBONs. Our data therefore suggest that fly memories are formed by dopamine-directed plasticity at cholinergic KC-MBON synapses.

RESULTS

Drosophila Kenyon Cell Function Requires ChAT Expression

Cholinergic neurons express ChAT to synthesize ACh and the vesicular ACh transporter (VAChT) that loads ACh into synaptic vesicles. Although prior studies concluded that KCs do not express ChAT (Gorczyca and Hall, 1987; Buchner et al., 1986; Yasuyama et al., 1995b), data from a microarray-based characterization of MB-expressed genes (Perrat et al., 2013) revealed levels of ChAT and VAChT that are not lower than elsewhere in the brain (*ChAT*: γ = 8.83, α′β′ = 8.43, αβ = 6.74, rest = 8.86, all p [neurons to rest of brain] > 0.05; *VAChT*: γ = 7.27, α′β′ = 5.94, αβ = 5.89, rest = 7.00, all p [neurons to rest of brain] > 0.05; t test). We therefore reinvestigated *ChAT* and *VAChT* expression in the MB using immunohistochemistry (Figures 1A and 1B; see Figure S1 and Movie S1 available online). We controlled for antibody specificity by staining brains expressing an UAS-*ChAT*^{RNAi} or UAS-*VAChT*^{RNAi} transgene driven in KCs by OK107-GAL4. Levels of ChAT staining appeared lower in the MB than in surrounding areas, consistent with prior studies (Gorczyca and Hall, 1987; Yasuyama et al., 1995b). However, ChAT immunoreactivity in the MB was above that in other areas of the brain, and MB labeling was significantly reduced in flies expressing UAS-*ChAT*^{RNAi} in KCs (Figures 1A and 1B). In comparison, VAChT immunoreactivity in the MB was at a similar level to other brain regions, and was significantly reduced when UAS-*VAChT*^{RNAi} was expressed

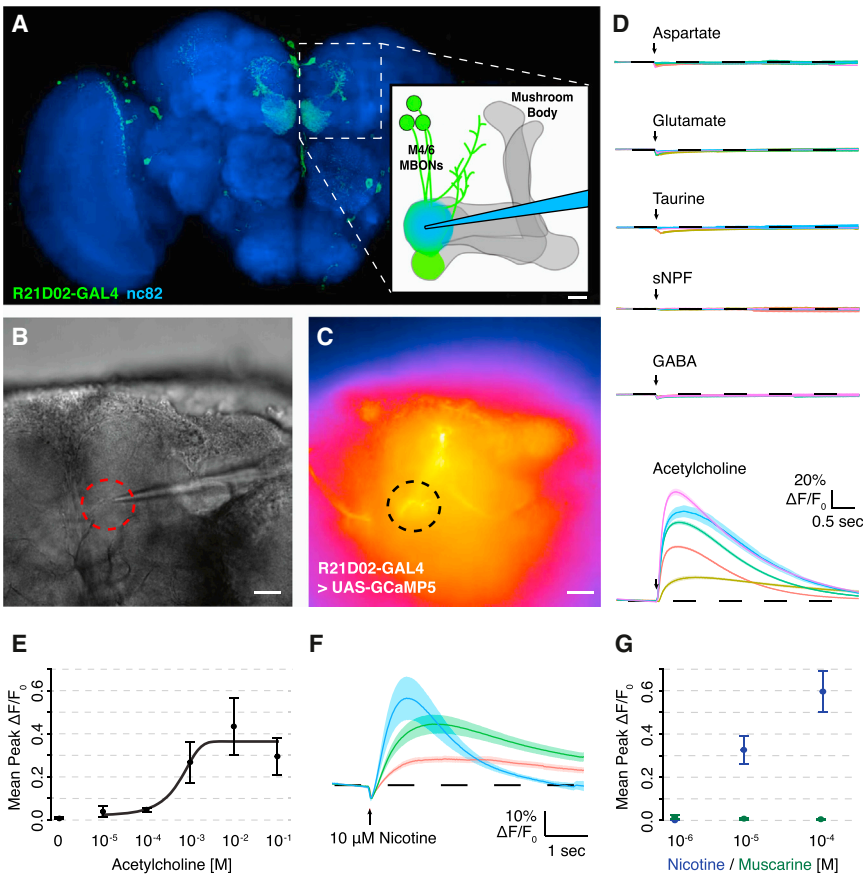

Figure 2. ACh Evokes Calcium Transients in M4/6 Neuron Dendrites

(A) Schematic of experimental setup. A micropipette connected to a pressure ejection system is placed near the dendrites of M4/6 MBONs in the tip of the horizontal MB lobe. M4/6 neural activity is monitored using R21D02-GAL4 (enhancer fragment from the *Dα6* locus)-driven UAS-GCaMP. Brain shown is costained with anti-Bruchpilot, a general neuropil marker (Wagh et al., 2006).

(B) Bright-field image of sample explant brain and micropipette. Region of interest (ROI) from which calcium traces were extracted is marked with a red dashed circle.

(C) Pseudocolor fluorescence image of the same area as in (B).

(D) Direct application of 1 mM of each candidate KC transmitter to M4/6 dendrites reveals activation by ACh only. n = 5 brains for each transmitter with ten trials per brain). Each colored trace represents an individual brain with the solid line representing the mean, and the shade representing the SEM.

(E) Dose-response curve of ACh responses (n = 5 brains per concentration). The line is a sigmoidal fit to the data. Data in (A)–(E) were acquired from R21D02-GAL4; UAS-GCaMP5 brains.

(F) Application of 10 μM nicotine elicits strong calcium responses in M4/6 dendrites. n = 3 brains; each colored line represents an individual brain. Solid line is the mean of five trials and shade the SEM.

(G) Calcium responses to increasing nicotine concentrations. No change is registered after applying muscarine. n = 3 brains each condition, mean of three trials. Data in (F) and (G) were acquired from R21D02-GAL4;UAS-GCaMP6f brains. Scale bar in (A)–(C), 20 μm. See Figure S3 for additional experiments. Error bars in (E) and (G) represent SEM.

in KCs (Figures 1A and 1B). Interestingly, levels of ChAT immunoreactivity were also reduced in the MB in UAS-*VAChT*^{RNAi}; OK107-GAL4 flies, suggesting an interaction between VAChT function and ChAT levels (Figures 1A and 1B). We therefore conclude that KCs express ChAT and VAChT, and that KCs, and not extrinsic neurons, are likely to provide the only cholinergic processes in the MB lobe region.

To test the functional relevance of ChAT and VAChT expression in KCs, we assessed the consequence of *ChAT*^{RNAi} and *VAChT*^{RNAi} disruption in aversive olfactory learning (Tully and Quinn, 1985). Three-minute aversive memory performance of *ChAT*^{RNAi};OK107 and *VAChT*^{RNAi};OK107 flies was statistically different from OK107-GAL4 and the relevant UAS-RNAi flies (Figure 1C). *VAChT*^{RNAi};OK107 flies also exhibited defective appetitive memory (Figure S2A). We expect the partial defect results from residual ChAT and VAChT activity. An early study with conditional *ChAT*^{ts} mutants concluded that normal fly behavior required only 8% of wild-type ChAT activity (Greenspan, 1980). We also tested for a role of GABAergic and glutamatergic transmission from KCs. Flies expressing RNAi against glutamic acid decarboxylase (GAD), the vesicular GABA transporter (vGAT), or the vesicular glutamate transporter (vGlut), driven by OK107-GAL4, had aversive memory performance that was statistically indistinguishable from controls (Figure S2B). We therefore conclude that KC function requires ACh.

ACh Evokes Responses in M4/6 MBONs

Postsynaptic MBONs should respond to ACh if it is a KC neurotransmitter. We therefore used the R21D02-GAL4 driver (Owald et al., 2015) to express the genetically encoded calcium indicator UAS-GCaMP (Akerboom et al., 2012; Chen et al., 2013) and monitored physiological responses to candidate transmitter application (Figure 2A). Brains were removed from R21D02-GAL4;UAS-GCaMP flies and placed on a polylysine-coated glass slide bathed with saline under a wide-field fluorescence microscope. 1 mM of glutamate, aspartate, taurine, sNPF, ACh, or GABA was then locally applied to the dendrites of M4/6 neurons via a glass micropipette using fast pressure ejection (Figures 2B–2D). Only ACh evoked a reproducibly robust increase in intracellular Ca^{2+} in M4/6 dendrites, and a dose response analysis revealed that 10 mM ACh application was sufficient to generate maximal signal (Figure 2E).

Since the KCs are principally driven by cholinergic olfactory projection neurons, we performed experiments to rule out the possibility that the M4/6 responses resulted from indirect activation of KCs. We first included 1 μM tetradotoxin (TTX) in the recording chamber to block voltage-gated sodium channels and thereby inhibit indirect activation through other neurons, and monitored the approximate diffusion of the ejected solution by including Texas red in the micropipette

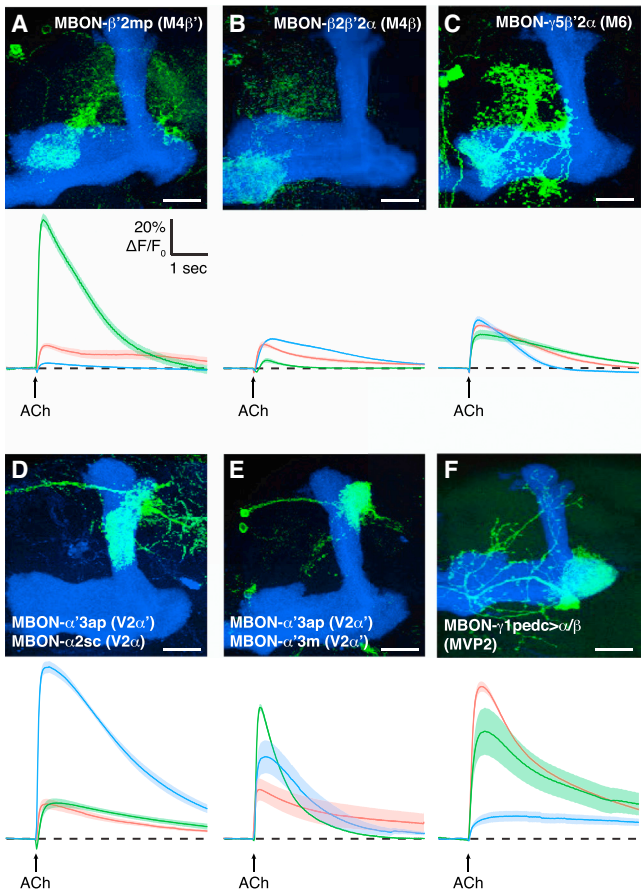

Figure 3. ACh Evokes Responses in Multiple Classes of MBONs

(A–F) Release of ACh onto the dendrites of other MBONs evokes calcium responses. Each panel shows the anatomy of the relevant MBON and below the corresponding GCaMP6f measured physiological responses evoked by 1 mM ACh.

(A–C) Glutamatergic MBONs on the horizontal MB lobe. (A) MBON-β′2mp (M4β′)/R39A05-GAL4, (B) MBON-β2β′2a (M4β)/R56F01-GAL4, and (C) MBON-γ5β′2a (M6)/R66C08-GAL4.

(D and E) Cholinergic MBONs on the vertical MB lobe. (D) MBON-α′3ap (V2α′), MBON-α2sc (V2α)/MB549C, (E) MBON-α′3ap (V2α′), MBON-α′3m (V2α′)/R24H08-GAL4.

(F) GABAergic MBON in the heel region, MBON-γ1pedc>αβ (MVP2)/MB112C. Each colored line represents the mean of ten trials per individual brain, and the shade represents the respective SEM (three brains per genotype). Scale bar, 20 μm. See Figure S4 for additional examples.

(Figure S3A). Visualizing Texas red fluorescence confirmed that activation was local, with the observed activity following the diffusing ACh. We next placed the micropipette tip in different locations with respect to the M4/6 dendrites to test whether more distant application of 100 μM ACh could evoke responses in M4/6 neurons. Maximal responses were only observed when ACh was released local to M4/6 dendrites (Figures S3B–S3D). We also challenged a potentially polysynaptic response by adding high extracellular Mg^{2+} to reduce the efficacy of synaptic transmission. Application of ACh to M4/6 dendrites of brains immersed in saline with high Mg^{2+} (+10 mM) generated responses that were not different to those evoked in low Mg^{2+} (Figure S3E). Importantly, high Mg^{2+} saline impaired the polysynaptic input to M4/6 neurons generated by stimulating KCs with ACh application in the MB calyx (Figure S3E). Finally, local ACh application to the MB lobes did not elicit Ca^{2+} transients in KCs (Figure S3F).

The relatively fast ACh-evoked response suggested that it involved nicotinic ACh receptors (nAChRs). We first tested this model by replacing ACh in the micropipette with 1, 10, or 100 μM of nicotine and applying it to the dendrites of M4/6 neurons (Figures 2F and 2G). Both 10 and 100 μM nicotine evoked robust responses in the M4/6 MBONs that were greater than those evoked by 100 μM ACh. In contrast, muscarine that should activate metabotropic AChRs did not elicit calcium transients at any concentration tested (Figures 2F and 2G). The nonselective nicotinic receptor antagonists mecamylamine (Figures S5A–S5D), hexamethonium (Figures S5G and S5H), and methyllycaconitine (MLA; Figures S5I and S5J) abolished ACh-evoked responses when added to the recording chamber, whereas vehicle had no effect (Figures S5E and S5F). Taken together, these experiments suggest that ACh directly activates M4/6 neurons via nAChRs.

Other MBONs Respond to ACh

We next tested whether other MBONs that are postsynaptic in the horizontal or vertical MB lobes responded to ACh. We restricted expression of GCaMP to a collection of these MBONs using specific GAL4 drivers (Aso et al., 2014b) and locally applied 1 mM ACh to their dendrites in the explant brain preparation (Figures 3A–3F and S4), starting with lines that label single M4/6 neurons. All of the MBONs tested responded to ACh application. This set of MBONs innervates all five of the major MB lobes (α, α′, β, β′, and γ) and represents all three of the characterized glutamatergic, cholinergic, and GABAergic classes of MBONs (Aso et al., 2014b). Although MBONs appeared to respond with distinct kinetics, we cannot currently exclude that differences result from placement of the micropipette. Nevertheless, multiple MBONs respond to ACh, consistent with ACh being released from all KC collaterals.

Optogenetic KC Activation Drives MBONs via nAChRs

To directly demonstrate that KCs are the source of ACh, we optogenetically activated them while recording calcium transients in M4/6 neuron presynaptic boutons using two-photon microscopy. We expressed lexAop-CsChrimson (Klapoetke et al., 2014) in KCs with 247-LexA::VP16 (Pitman et al., 2011) control and evoked activity using a focused red light emitting diode (Figures 4A–4F). Recording with two-photon illumination should minimize nonspecific activation of the Channelrhodopsin in these experiments. As expected (Owald et al., 2015), KC activation evoked intracellular Ca^{2+} transients in M4/6 neurons that were tightly temporally linked to the illumination protocol (Figures 4A–4F). Importantly, these optogenetically evoked M4/6 responses were also blocked by adding 250 μM mecamylamine (Figures 4A–4C), but not vehicle (Figures 4D–4F; Movie S2), to the recording chamber. Comparison of the average peak calcium response from four trials before and after application of mecamylamine or vehicle only revealed a significant difference for the mecamylamine group (Figures 4C and 4F). Importantly,

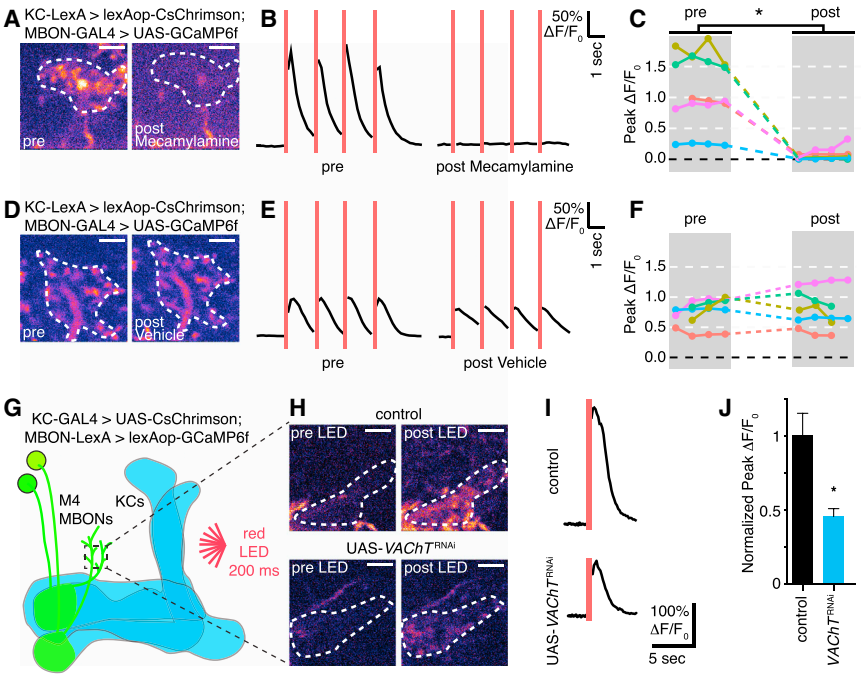

Figure 4. Optogenetic Activation of KCs Evokes ACh-Dependent Calcium Responses in M4/6 Neurons

(A–F) Optogenetic stimulation of KCs triggers M4/6 calcium responses that are blocked by mecamylamine. 247-LexA-driven lexAop-CsChrimson was used to activate KCs, and M4/6 neuron calcium transients were monitored with R21D02-GAL4 driven UAS-GCaMP6f.

(A) Samples of two-photon images of M4/6 presynaptic arbors collected on the first frame after LED stimulation, before and after mecamylamine application. Dotted white circle represents ROI from which $\Delta F/F_0$ is calculated.

(B and C) A total of 200 ms of red LED light (indicated by red vertical lines) triggers strong calcium responses in M4/6 neuron axons that are abolished 5 min after applying 250 μM mecamylamine.

(B) Sample trace and (C) quantification, n = 5 brains, asterisk denotes $p < 0.05$, paired samples t test.

(D) KC-evoked M4/6 neuron responses remain stable after application of vehicle.

(E and F) (E) Sample trace and (F) quantification, n = 5 brains, $p > 0.05$, paired samples t test. See Figure S5 for washout experiments and others using 100 μM mecamylamine or additional nicotinic antagonists.

(G–J) KC-expressed UAS-*VAChT*^{RNAi} reduces KC-triggered M4 calcium responses. (G) Illustration of experimental setup. R13F02-GAL4-driven UAS-CsChrimson was used to optogenetically activate KCs while M4 calcium transients were monitored with R15B01-LexA driven lexAop-GCaMP6f. (H) Samples of two-photon images of M4 presynaptic arbors collected before and after LED stimulation in control brains (upper panel) or those coexpressing UAS-*VAChT*^{RNAi} in KCs (lower panel). Dotted white circles represent ROI from which $\Delta F/F_0$ is calculated. (I and J) A total of 200 ms of red light evokes calcium responses in presynaptic arbors of M4 neurons that have a significantly reduced peak when *VAChT*^{RNAi} is coexpressed in KCs. (I) Sample trace and (J) quantification, n = 4–6 brains, asterisk denotes $p < 0.05$, Mann-Whitney U-test. Data are normalized to controls. Scale bars, 5 μM. Error bars represent SEM.

the mecamylamine effect was reversed following washout (Figures S5K–S5N). Consistent with prior studies (Mauss et al., 2014), 100 μM mecamylamine did not abolish responses in this preparation but caused a strong and reversible reduction (Figures S5K and S5L).

We also tested whether reducing VAChT expression in KCs attenuated M4/6 MBON responses. We coexpressed UAS-*VAChT*^{RNAi} and UAS-CsChrimson in KCs with R13F02-GAL4 and lexAop-GCaMP6f in M4 neurons with R15B01-LexA. Strikingly, peak KC-evoked responses were reduced by greater than 50% in flies expressing UAS-*VAChT*^{RNAi} in KCs (Figures 4G–4J). Therefore pharmacological and genetic approaches provide evidence that the KCs release ACh that in turn activates M4/6 MBONs via nAChRs.

Manipulating nAChR Expression in M4/6 MBONs Phenocopies Neural Blockade

We next tested whether downregulating specific nAChR subunits altered odor-evoked responses in M4/6 neurons. We used R21D02-GAL4 to coexpress UAS-GCaMP6f and UAS-RNAi constructs directed toward the Dα1, Dα3, Dα4, Dα5, or Dα6 nAChR subunits. Living flies were mounted under the two-photon microscope, and MCH and OCT odor responses were recorded from M4/6 presynaptic boutons. Expression of *Dα1*, *Dα4*, *Dα5*, and *Dα6* subunit RNAi caused a statistically significant reduction in the peak responses to MCH, as compared to controls (Figures 5A and 5B). *Dα4* and *Dα6* RNAi also significantly reduced the responses to OCT. In comparison, *Dα3* RNAi peak responses were indistinguishable from those of controls for both odors (Figure 5B).

We reasoned that reducing expression of the relevant nicotinic acetylcholine receptor subunits in M4/6 MBONs might also alter odor-driven behavior (Figure 5C). Previous work showed that blocking M4/6 neuron output with VT1211-GAL4-driven UAS-*Shibire*^{ts1} converted naive odor avoidance into odor approach (Owald et al., 2015). We therefore used this assay to assess the role of Dα1, Dα3, Dα4, Dα5, and Dα6 subunits in M4/6 MBONs. Flies were given the choice between a T-maze arm perfused with a 1:1,000 dilution of MCH and an arm with a clean air stream. Whereas control VT1211-GAL4/+ or UAS-RNAi/+ flies displayed MCH avoidance or neutrality, flies expressing UAS-*Dα1*, *Dα4*, *Dα5*, or *Dα6* RNAi in M4/6 MBONs exhibited a significant reversal of odor driven behavior. Flies expressing *Dα3* RNAi were not statistically different from relevant controls. These behavioral phenotypes mirror the defective MCH-evoked physiological responses and resemble the reversal of naive odor behavior observed when M4/6 neurons were blocked (Owald et al., 2015). We therefore conclude that M4/6 neurons are principally driven by KCs via ACh neurotransmission onto nAChRs.

sNPF Potentiates ACh-Evoked Responses in MBONs

The αβ and γ KCs express the sNPF neuropeptide (Johard et al., 2008), and reducing sNPF expression in KCs impairs appetitive memory (Knapek et al., 2013). Finding a role for ACh as a key

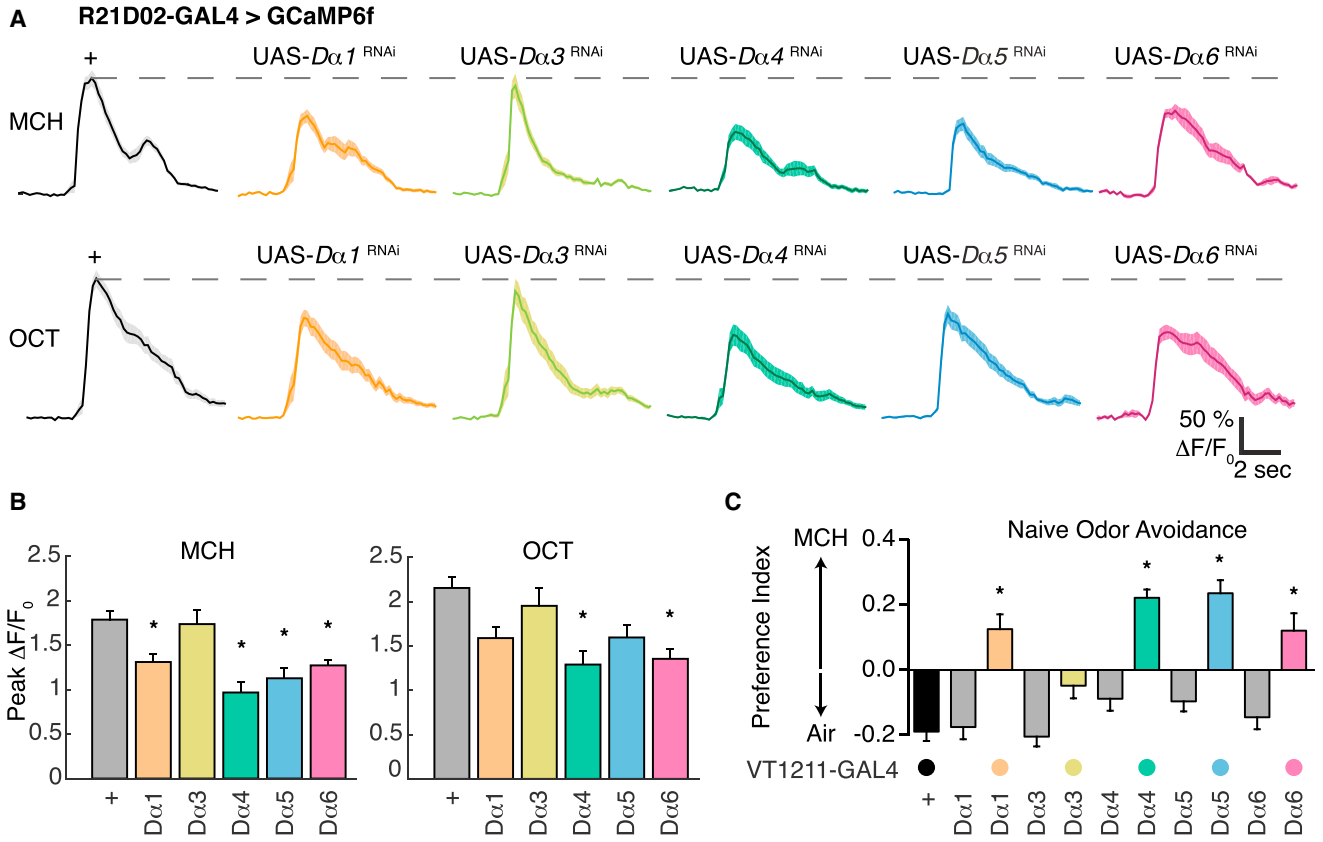

Figure 5. Reducing nAChR Subunit Expression in M4/6 MBONs Impairs Physiological and Behavioral Odor-Evoked Responses

(A) nAChR subunit expression is required for MCH- and OCT-evoked calcium transients in M4/6 neuron axons. Mean traces of activity evoked by 5 s of odor presentation, with SEM as shade (n = 9–16 from 5–10 animals). Head-fixed live flies carrying R21D02-GAL4-driven UAS-GCaMP6f show robust calcium responses to MCH and OCT odors that are impaired by expressing nAChR-directed RNAi.

(B) Quantification of peak calcium responses in (A). MCH-evoked responses are significantly reduced in flies expressing UAS-*Dα1*^{RNAi}, UAS-*Dα4*^{RNAi}, UAS-*Dα5*^{RNAi}, and UAS-*Dα6*^{RNAi} (n = 9–16, asterisk denotes $p < 0.05$, one-way ANOVA with Dunnett's multiple comparisons test). OCT-evoked responses are significantly reduced in flies expressing UAS-*Dα4*^{RNAi} and UAS-*Dα6*^{RNAi} (n = 9–16, asterisk denotes $p < 0.05$, one-way ANOVA with Dunnett's multiple comparisons test).

(C) nAChR RNAi in M4/6 neurons phenocopies the behavioral consequence of neural blockade. Flies were given 2 min in a T maze to choose between a tube perfused with 1:1,000 MCH and another with clean air. VT1211-GAL4;UAS-*Dα1*^{RNAi}, VT1211-GAL4;UAS-*Dα4*^{RNAi}, VT1211-GAL4;UAS-*Dα5*^{RNAi}, and VT1211-GAL4;UAS-*Dα6*^{RNAi} exhibit a significant preference toward MCH when compared to their two respective genetic control groups (n = 18–38, asterisk denotes $p < 0.001$, one-way ANOVA with Tukey's multiple comparisons test). Error bars in (B) and (C) represent SEM.

fast-acting transmitter between KCs and MBONs raises the question of whether coreleased sNPF and ACh interact. We therefore coapplied ACh and sNPF with a micropipette to the M4/6 dendrites in the explant brain preparation, while monitoring calcium transients by wide-field imaging (Figure 6). Calcium transients evoked in M4/6 MBONs by dual ACh and sNPF application were significantly larger than those generated by ACh and vehicle, supporting a likely facilitating interaction between the slow- and fast-acting transmitters.

DISCUSSION

Despite decades of work on learning and memory and other functions of the MB, the identity of the fast-acting neurotransmitter that is released from the KCs has remained elusive. Much of the insect brain was considered to be cholinergic, but the MB was thought to be unique. Histological studies concluded that the MB did not express ChAT (Gorczyca and Hall, 1987; Buchner et al., 1986; Yasuyama et al., 1995b) but that subsets of KCs contained glutamate, aspartate, or taurine (Sinakevitch et al., 2001; Strausfeld et al., 2003). However, conclusive evidence that these molecules are released as neurotransmitters has not materialized.

Here we present multiple lines of evidence that ACh is a KC transmitter. (1) KCs express the ChAT and VAChT proteins that synthesize and package ACh into synaptic vesicles, and the expression of these genes is required for MB-dependent learned behavior. (2) Stimulation of KCs triggers responses in MBONs that are similar to those evoked by direct ACh application. (3) Reducing ACh processing in KCs impairs KC-evoked responses in MBONs. (4) ACh- and KC-evoked responses in MBONs are both sensitive to antagonism of nicotinic ACh

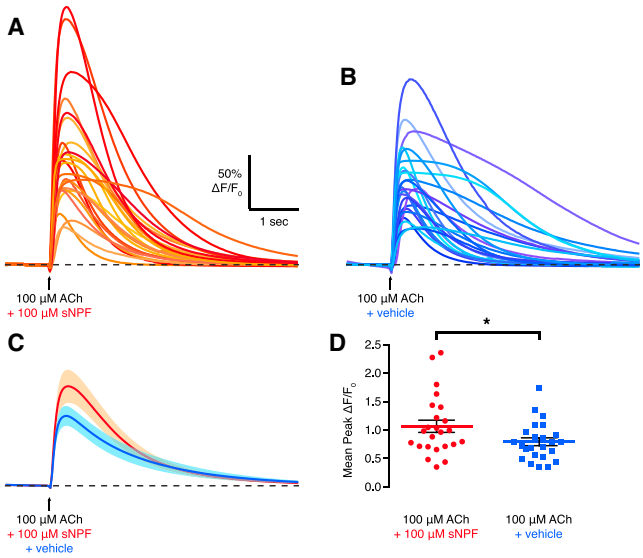

Figure 6. sNPF Increases ACh-Evoked Calcium Transients in M4/6 Neurons

A total of 100 μM of ACh was applied through a micropipette onto the M4/6 dendrites, with either 100 μM sNPF or vehicle. Calcium transients were measured from M4/6 dendrites of R21D02-GAL4; UAS-GCaMP6f explant brains.

(A and B) Mean calcium traces of ten trials from 24 brains per condition.

(C) Overlaid mean traces from (A) ACh plus sNPF and (B) ACh plus vehicle. Shade represents SEM.

(D) Mean peak calcium responses are significantly higher when ACh is coapplied with 100 μM sNPF than with vehicle ($t[39.09] = 2.12$, $p < 0.05$, unpaired t test with Welch's correction). Error bars represent SEM.

receptors. (5) Odor-evoked responses in MBONs are attenuated by reducing the expression of several nicotinic ACh receptor subunits. Taken together, these data provide compelling support that ACh is a major neurotransmitter released from *Drosophila* KCs.

The anatomy of ACh-responsive MBONs suggests that many αβ, α′β′, and γ lobe KCs are likely to be cholinergic. Calcium imaging may miss subtle or inhibitory effects, so it remains possible that subclasses of KC might also release or corelease other small molecule transmitters. It is, for example, notable that the MB neurons express an atypical putative vesicular transporter (Brooks et al., 2011). Furthermore, taurine histology specifically labels the αβ core neurons (Strausfeld et al., 2003). Anatomy suggests that αβ core and αβ surface outputs are pooled by MBONs with dendrites in the α lobe tip and throughout the β lobe, but that the dendrites of MBONs in the α lobe stalk preferentially innervate αβ surface neurons (Perisse et al., 2013b). It will be important to understand how ACh signals from different KCs are integrated by MBONs. The αβ and γ, but not α′β′, KCs can corelease ACh with the sNPF neuropeptide (Johard et al., 2008). Our data raise the possibility that coreleased sNPF may facilitate ACh-evoked responses. sNPF drives autocrine presynaptic facilitation of certain olfactory sensory neurons in the adult fly (Root et al., 2011). Conversely, sNPF decreased the resting membrane potential of larval motor neurons that ectopically express sNPFR (Vecsey et al., 2014). MBONs with dendrites in certain lobes therefore receive different combinations of transmitters and may vary in responding to sNPF.

Finding that ACh is the KC transmitter has important implications for learning-relevant plasticity at KC-MBON synapses. Current models suggest that valence-specific and anatomically restricted reinforcing dopaminergic neurons drive presynaptically expressed plasticity between KCs and particular MBONs (Waddell, 2013; Aso et al., 2014a; Aso et al., 2014b; Owald et al., 2015; Owald and Waddell, 2015). Reward learning skews KC-MBON outputs toward driving approach by depressing the odor drive to MBONs that direct avoidance, whereas aversive learning enhances drive to avoidance by reducing drive to approach MBONs and increasing drive to avoidance pathways (Owald et al., 2015; Owald and Waddell, 2015). The results here indicate that learning is represented as dopaminergic tuning of excitatory cholinergic KC-MBON synapses.

Learning requires dopamine receptor function in the KCs (Kim et al., 2007; Qin et al., 2012), which implies a presynaptic mechanism of plasticity at the KC-MBON junction. Presynaptic plasticity of odor-activated KCs provides a simple means to retain odor specificity of memory in the highly convergent anatomy of the MB—where 2,000 KCs converge onto single or very few MBONs per zone on the MB lobes. The anatomically analogous mammalian cerebellar circuits, to which the insect MBs have been compared (Farris, 2011), exhibit presynaptic glutamatergic plasticity that is cAMP dependent (Salin et al., 1996). Finding that the KC transmitter is ACh suggests that cAMP-dependent mechanisms can modulate synaptic connections, regardless of transmitter identity. The MB KCs appear to be strikingly similar to the large parallel ensemble of cholinergic amacrine cells in the vertical lobe of the cuttlefish (Shomrat et al., 2011). These Cephalopod amacrine cells also share the same fan-out input and fan-in efferent anatomy of the *Drosophila* KCs, and plasticity occurs at the cholinergic connection between amacrine cells and downstream large efferent neurons.

Work in the locust suggested that spike-timing-dependent plasticity (STDP) marks the relevant conditioned odor-activated KC-MBON synapses so that they are susceptible to reinforcing modulation (Cassenaer and Laurent, 2012). STDP relies on coincidence of pre- and postsynaptic activity and influx of postsynaptic Ca^{2+} through NMDA-type glutamate receptors (Feldman, 2012). Recent work in *Drosophila* pairing odor presentation with dopaminergic neuron activation reported odor-specific synaptic depression at a KC-MBON junction that did not require postsynaptic MBON depolarization (Hige et al., 2015). It will be important to determine whether this holds for all DAN-MBON compartments or whether some learning-induced plasticity involves synaptic Ca^{2+} influx through an ACh-triggered nAChR, rather than the more traditional glutamate-gated NMDA receptors.

We identified roles for the Dα1, Dα4, Dα5, and Dα6 nAChR subunits in M4/6 MBONs. Reducing the expression of these subunits lowered odor-evoked signals in MBONs and converted naive odor avoidance into approach behavior. Dα5 and Dα6 subunits can form functional heteromeric channels in vitro (Lansdell et al., 2012). Different MBONs may express unique combinations of AChRs (Le Novère et al., 2002; Chamaon et al., 2002; Thany et al., 2007) and therefore have characteristic physiological

responses to KC-released ACh, as well as perhaps different learning rules and magnitudes of plasticity (Hige et al., 2015). Pre- or postsynaptically localized muscarinic AChRs could provide additional memory-relevant modulation.

Beyond important roles in memory formation, consolidation, and expression, the MB- and DAN-directed modulation of specific MBON pathways has also been implicated in controlling hunger, thirst, temperature, and sleep/wake state-dependent locomotor behaviors (Krashes et al., 2009; Lewis et al., 2015; Lin et al., 2014b; Shih et al., 2015; Sitaraman et al., 2015). It will therefore be important to understand how plasticity of cholinergic KC transmission serves these discrete functions.

EXPERIMENTAL PROCEDURES

Fly Strains

Flies for physiological experiments were reared in vials with standard cornmeal food with additional molasses and active dried yeast. Flies for behavior were raised in bottles with standard cornmeal food. Canton-S flies were the wild-type control. We used Split-GAL4 lines MB002B, MB011B, MB027B, MB112C, MB210B, and MB549C (Aso et al., 2014a) and GAL4 lines R13F02 (Jenett et al., 2012), R21D02 (Jenett et al., 2012; Owald et al., 2015), R24H08, R39A05, R56F01, R66C08, R93F01 (Jenett et al., 2012), OK107 (Connolly et al., 1996), and VT1211 (Owald et al., 2015). We also used LexA lines R15B01 (Jenett et al., 2012; Lewis et al., 2015) and 247-LexA::VP16 (Pitman et al., 2011). UAS-GCaMP5 (Akerboom et al., 2012), UAS-GCaMP6f, and LexAop-GCaMP6f (Chen et al., 2013) were used for calcium imaging. UAS-CsChrimson and lexAop-CsChrimson (Klapoetke et al., 2014) were the optogenetic activators. Prior to optogenetic experiments, all flies were housed on standard cornmeal food with 1 mM retinal for 1–3 days. RNAi lines were UAS-*ChAT*^{RNAi} (Bloomington BUN 25856) (Ni et al., 2009), UAS-*VAChT*^{RNAi} (VDRC ID 27684), UAS-*GAD*^{RNAi} (VDRC ID 32344), UAS-*VGAT*^{RNAi} (VDRC ID 103586), UAS-*VGlut*^{RNAi} (VDRC ID 104324) (Dietzl et al., 2007), and UAS-*nAChR*^{RNAi} (Bloomington BUNs 28688, 27671, 31985, 25943, and 25835) (Ni et al., 2009).

Pharmacology

All candidate neurotransmitters, agonists, and antagonists, except sNPF, were prepared in adult hemolymph-like saline, AHLS (Wang et al., 2003; 2 mM $CaCl_2$, 5 mM KCl, 8.2 mM $MgCl_2$, 108 mM NaCl, 4 mM $NaHCO_3$, 1 mM NaH_2PO_4, 10 mM sucrose, and 5 mM trehalose) to a concentration of 100 mM. Aspartate, glutamate, taurine, GABA, ACh, nicotine, muscarine, mecamylamine, methyllycaconitine, and hexamethonium were all from Sigma Aldrich. Short neuropeptide F (sNPF; Ala-Gln-Arg-Ser-Pro-Ser-Leu-Arg-Leu-Arg-Phe-NH_2) was synthesized by PolyPeptide (Strasbourg, France) to a purity of >95% and was dissolved in DMSO. Each solution delivered in the micropipette also contained 5 μM Texas red dextran (TXR; Life Technologies) to monitor diffusion.

Explant Brain Wide-Field Calcium Imaging

All micropipette ejection experiments were performed on explant brains using wide-field imaging. One- to seven-day-old flies were anesthetized on ice, and brains were dissected in calcium-free AHLS and imaged in AHLS. The pH was adjusted to 7.5 and osmolarity to 265 mOsm. Dissected brains were adhered to a polylysine-coated coverslip and were illuminated with an X-Cite 120PC Q arc lamp. Micropipettes (glass capillaries, Harvard Apparatus, 300092) with an opening diameter of approximately 3 μm were connected to a picospritzer III (Intracell). The tip of the pipette was positioned near the M4/6 dendrites in the tip of the MB horizontal lobes (Figure 2B), unless stated otherwise. A custom white LED provided a stimulus trigger signal 1 s before stimulation. Air pressure to the picospritzer was set to the minimum required to eject solution from the pipette. Release of solution was verified by applying small test pulses while observing TXR in the red fluorescence channel.

Image series were acquired using a Scientifica Slicescope with a 40×, 0.8 NA water-immersion objective and Andor Zyla sCMOS camera with Andor Solis software (v4.27). Time series were acquired at 33.3 Hz with 512 × 512 pixels and 16 bit (or 100 Hz for traces shown in Figure S3E). Experiments in Figures S3E and S3F were acquired with a Guppy Pro CCD camera (Allied) with AVT SmartView software (v1.14). These time series were acquired at 12 Hz with 640 × 480 pixels and 8 bit. Image stacks were subsequently analyzed in Matlab (Mathworks Inc.) using custom-written scripts. In brief, elliptical ROIs (e.g., Figure 2B) were manually drawn around M4/6 dendrites (unless stated otherwise), and the mean fluorescence F of this ROI was calculated for each image. The resulting trace was scanned for LED trigger signals, and individual $\Delta F/F_0$ response traces were extracted from 1 s before and 3–10 s after the stimulation trigger. F_0 was defined for each trial as the mean F from 1 s before stimulation up to the point of stimulation. The peak $\Delta F/F_0$ was obtained by taking the maximum $\Delta F/F_0$ value acquired between the time of the trigger signal and 3 s afterward. Neural responsiveness was verified by applying 500 mM KCl at the end of each experiment.

Explant Brain Two-Photon Calcium Imaging

Combined optogenetic and calcium imaging experiments were conducted using a two-photon microscope (Scientifica) to minimize inadvertent optogenetic stimulation through imaging light. Explant brains were bathed in carbogenated (95% O_2, 5% CO_2) buffer solution (103 mM NaCl, 3 mM KCl, 5 mM N-Tris, 10 mM trehalose, 10 mM glucose, 7 mM sucrose, 26 mM $NaHCO_3$, 1 mM NaH_2PO_4, 1.5 mM $CaCl_2$, 4 mM $MgCl_2$, osmolarity 275 mOsm [pH 7.3]) following dissection in calcium-free buffer. For light stimulation, we used a high-power LED (Multicomp OSW-6338, 630 nm) relayed onto the specimen via a 50 mm diameter lens with focal length 60 mm. The power at the specimen was measured to be 0.85 mW/mm^2. The LED was triggered using a microcontroller (Arduino MEGA). Light pulses were delivered at 40 Hz, with 10 ms duration for a total of 200 ms per stimulation.

Fluorescence was excited using 140 fs pulses, 80 MHz repetition rate, centered on 910 nm generated by a Ti-Sapphire laser (Chameleon Ultra II, Coherent). Images of 256 × 256 pixels were acquired at 5.92 Hz, controlled by ScanImage 3.8 software (Pologruto et al., 2003). Two-photon fluorescence images were manually segmented using ImageJ and further analyzed using the custom-written MATLAB scripts described above.

For washout experiments, explant brains were continuously perfused with carbogenated buffer at about 2 ml/min using a Watson-Marlow 120S/DV WM Sci Q400-1H1D perfusion system. Antagonist action was measured 5 min after addition to the bath, followed by washout. The result of washout was measured 30 min later.

In Vivo Two-Photon Calcium Imaging

Two-photon imaging of odor-evoked calcium responses was performed according to Owald et al. (2015). Three- to eight-day-old flies were briefly anesthetized on ice and mounted in a custom chamber. The head capsule was opened under room temperature carbogenated buffer (see above). The legs and proboscis were immobilized with wax. Odors were delivered on a clean air carrier stream using a custom-designed system (Shang et al., 2007), which also synchronizes the timing of odor delivery and the two-photon image acquisition. Two-photon fluorescence images were manually segmented using ImageJ. Movement of the animal was small enough such that images did not require registration. Where possible, each hemisphere was separately evaluated and treated as an independent "n." All subsequent analyses utilized custom-written Matlab routines. After applying test pulses, flies were exposed to 5 s MCH (air stream passing over 10^{-2} odor dilution in mineral oil, and then further blended 1:9 with a clean air stream), then 15 s clean air, followed by a 5 s OCT pulse. Peaks were taken as maximum $\Delta F/F_0$ between 1 and 2 s after the beginning of odor stimulation. F_0 was defined as the mean F from 2 s before odor stimulation to the beginning of stimulation.

Immunohistochemistry

Brains were dissected on ice, fixed in 4% paraformaldehyde, and stained according to Wu and Luo (2006). For ChAT and VAChT staining, brains were incubated in PBT (0.3% Triton) supplemented with anti-ChAT primary mouse antibody (Yasuyama et al., 1995a) (diluted 1:100) and anti-VAChT primary rabbit antibody (Kitamoto et al., 1998) (diluted 1:1,000) for 2 days, followed by

2 days' incubation with secondary antibodies (anti-mouse Alexa 488/anti-rabbit Alexa 546, Sigma). For GAL4 visualization, anti-GFP (rabbit, Invitrogen, dilution 1:100) and anti-nc82 (DSHB, dilution 1:50) were used as primary antibodies. All confocal images were acquired on a Leica SP5 at manually adjusted laser intensity and gain. The same settings were used for all brains when comparing ChAT/VAChT antibody label.

For antibody quantification, a defined rectangular ROI of approximately 40 × 25 μm was placed over a single frame of the gamma lobe as well as the superior medial protocerebrum (SMP), the mean fluorescence was assessed using ImageJ, and each brain's gamma lobe intensity was normalized to the respective SMP intensity, individually for each channel.

Behavior

Mixed-sex populations of 4- to 9-day-old flies were tested together in all memory experiments. Aversive training was performed as in Perisse et al. (2013b). Briefly, flies were exposed to CS+ for 1 min with 12 90 V electric shocks at 5 s intervals followed by 45 s of air and the CS− for 1 min. For testing, flies were given 2 min to choose between the CS+ and CS− in a T maze. Performance index (PI) was calculated as the number of flies in the conditioned odor, minus the number of flies going the other direction, divided by the total number of flies in the experiment. A single PI value is the average score from flies of the identical genotype tested with the reciprocal reinforced/nonreinforced odor combination (Tully and Quinn, 1985; Perisse et al., 2013b). Odor dilutions were adjusted between experiments and odor batches to minimize bias (MCH 5–8 μl in 8 ml mineral oil and OCT 7–8 μl in 8 ml mineral oil). Appetitive conditioning was performed as in Perisse et al. (2013b). Naive odor avoidance experiments were performed as in Owald et al. (2015). Briefly, 5-day-old flies starved for 21–24 hr were given 2 min to choose between MCH (diluted 1:1,000 in mineral oil) and mineral oil-suffused air streams. Preference index was calculated as the number of flies approaching the odor minus the number approaching mineral oil, divided by the total number of flies in the experiment. One "n" corresponds to a single test trial.

Statistics

Statistical analyses were performed in either Matlab, GraphPad Prism 6, or R. The sigmoid dose-response curve fit for ACh application was performed in GraphPad Prism, based on the average of three trials per brain, with five brains per condition. Effects of pharmacological treatments were investigated using a paired t test to compare the average response peak before and after application. Groups in antibody quantification and behavioral experiments were compared using one-way ANOVA followed by Tukey's multiple comparisons test. Dunnett's multiple comparisons test was used for $nAChR^{RNAi}$ odor-evoked calcium responses. The effects of $VAChT^{RNAi}$ on calcium response peaks were measured using the Mann-Whitney U-test for nonparametric data. Calcium responses in Figure 6 were compared using an unpaired t test with Welch's correction.

SUPPLEMENTAL INFORMATION

Supplemental Information includes five figures and two movies and can be found with this article at http://dx.doi.org/10.1016/j.neuron.2016.02.015.

AUTHOR CONTRIBUTIONS

O.B., D.O., and S.W. conceived the project and designed all experiments. O.B. performed and with D.O. analyzed all experiments, except behavior, which was performed by J.F. Imaging data were acquired using custom hardware and software designed by J.-P.M. and C.B.T. Microarray data were generated by P.N.P. Essential fly lines were constructed by R.B. The manuscript was written by S.W., D.O., and O.B.

ACKNOWLEDGMENTS

We thank G. Miesenböck, members of the Waddell and Miesenböck labs, and M. Dolan for support, technical help, and discussion. O.B. also thanks A. Petzold and Q. Geissmann. We are grateful to M. Landgraf, G. Rubin, and the Janelia FlyLight Project; B. Dickson and the VDRC; and the Bloomington stock center for fly lines. We also thank T. Kitamoto and the Iowa Developmental Studies Hybridoma Bank for antibodies. O.B. is funded by the Medical Research Council and a University College War Memorial Studentship. D.O. was supported by an EMBO Long-Term Fellowship and a Sir Henry Wellcome Postdoctoral Fellowship. J.F. is funded by the Deutsche Forschungsgemeinschaft (GZ:FE 1563/1-1). S.W. is funded by a Wellcome Trust Senior Research Fellowship in the Basic Biomedical Sciences and by funds from the Gatsby Charitable Foundation, the Oxford Martin School, and the Bettencourt-Schueller Foundation.

Received: July 22, 2015
Revised: January 4, 2016
Accepted: January 27, 2016
Published: March 3, 2016

REFERENCES

Akerboom, J., Chen, T.W., Wardill, T.J., Tian, L., Marvin, J.S., Mutlu, S., Calderón, N.C., Esposti, F., Borghuis, B.G., Sun, X.R., et al. (2012). Optimization of a GCaMP calcium indicator for neural activity imaging. J. Neurosci. *32*, 13819–13840.

Aso, Y., Herb, A., Ogueta, M., Siwanowicz, I., Templier, T., Friedrich, A.B., Ito, K., Scholz, H., and Tanimoto, H. (2012). Three dopamine pathways induce aversive odor memories with different stability. PLoS Genet. *8*, e1002768.

Aso, Y., Hattori, D., Yu, Y., Johnston, R.M., Iyer, N.A., Ngo, T.T., Dionne, H., Abbott, L.F., Axel, R., Tanimoto, H., and Rubin, G.M. (2014a). The neuronal architecture of the mushroom body provides a logic for associative learning. eLife *3*, e04577.

Aso, Y., Sitaraman, D., Ichinose, T., Kaun, K.R., Vogt, K., Belliart-Guérin, G., Plaçais, P.Y., Robie, A.A., Yamagata, N., Schnaitmann, C., et al. (2014b). Mushroom body output neurons encode valence and guide memory-based action selection in Drosophila. eLife *3*, e04580.

Blum, A.L., Li, W., Cressy, M., and Dubnau, J. (2009). Short- and long-term memory in Drosophila require cAMP signaling in distinct neuron types. Curr. Biol. *19*, 1341–1350.

Bouzaiane, E., Trannoy, S., Scheunemann, L., Plaçais, P.Y., and Preat, T. (2015). Two independent mushroom body output circuits retrieve the six discrete components of Drosophila aversive memory. Cell Rep. *11*, 1280–1292.

Brooks, E.S., Greer, C.L., Romero-Calderón, R., Serway, C.N., Grygoruk, A., Haimovitz, J.M., Nguyen, B.T., Najibi, R., Tabone, C.J., de Belle, J.S., and Krantz, D.E. (2011). A putative vesicular transporter expressed in Drosophila mushroom bodies that mediates sexual behavior may define a neurotransmitter system. Neuron *72*, 316–329.

Buchner, E., Buchner, S., Crawford, G., Mason, W.T., and Salvaterra, P.M. (1986). Choline acetyltransferase-like immunoreactivity in the brain of Drosophila melanogaster. Cell Tissue Res. *246*, 57–62.

Burke, C.J., Huetteroth, W., Owald, D., Perisse, E., Krashes, M.J., Das, G., Gohl, D., Silies, M., Certel, S., and Waddell, S. (2012). Layered reward signalling through octopamine and dopamine in Drosophila. Nature *492*, 433–437.

Campbell, R.A., Honegger, K.S., Qin, H., Li, W., Demir, E., and Turner, G.C. (2013). Imaging a population code for odor identity in the Drosophila mushroom body. J. Neurosci. *33*, 10568–10581.

Caron, S.J., Ruta, V., Abbott, L.F., and Axel, R. (2013). Random convergence of olfactory inputs in the Drosophila mushroom body. Nature *497*, 113–117.

Cassenaer, S., and Laurent, G. (2012). Conditional modulation of spike-timing-dependent plasticity for olfactory learning. Nature *482*, 47–52.

Chamaon, K., Smalla, K.H., Thomas, U., and Gundelfinger, E.D. (2002). Nicotinic acetylcholine receptors of Drosophila: three subunits encoded by genomically linked genes can co-assemble into the same receptor complex. J. Neurochem. *80*, 149–157.

Chen, T.W., Wardill, T.J., Sun, Y., Pulver, S.R., Renninger, S.L., Baohan, A., Schreiter, E.R., Kerr, R.A., Orger, M.B., Jayaraman, V., et al. (2013).

Ultrasensitive fluorescent proteins for imaging neuronal activity. Nature *499*, 295–300.

Claridge-Chang, A., Roorda, R.D., Vrontou, E., Sjulson, L., Li, H., Hirsh, J., and Miesenböck, G. (2009). Writing memories with light-addressable reinforcement circuitry. Cell *139*, 405–415.

Connolly, J.B., Roberts, I.J., Armstrong, J.D., Kaiser, K., Forte, M., Tully, T., and O'Kane, C.J. (1996). Associative learning disrupted by impaired Gs signaling in Drosophila mushroom bodies. Science *274*, 2104–2107.

Daniels, R.W., Gelfand, M.V., Collins, C.A., and DiAntonio, A. (2008). Visualizing glutamatergic cell bodies and synapses in Drosophila larval and adult CNS. J. Comp. Neurol. *508*, 131–152.

Das, G., Klappenbach, M., Vrontou, E., Perisse, E., Clark, C.M., Burke, C.J., and Waddell, S. (2014). Drosophila learn opposing components of a compound food stimulus. Curr. Biol. *24*, 1723–1730.

Dietzl, G., Chen, D., Schnorrer, F., Su, K.C., Barinova, Y., Fellner, M., Gasser, B., Kinsey, K., Oppel, S., Scheiblauer, S., et al. (2007). A genome-wide transgenic RNAi library for conditional gene inactivation in Drosophila. Nature *448*, 151–156.

Farris, S.M. (2011). Are mushroom bodies cerebellum-like structures? Arthropod Struct. Dev. *40*, 368–379.

Farris, S.M. (2013). Evolution of complex higher brain centers and behaviors: behavioral correlates of mushroom body elaboration in insects. Brain Behav. Evol. *82*, 9–18.

Feldman, D.E. (2012). The spike-timing dependence of plasticity. Neuron *75*, 556–571.

Galili, D.S., Dylla, K.V., Lüdke, A., Friedrich, A.B., Yamagata, N., Wong, J.Y., Ho, C.H., Szyszka, P., and Tanimoto, H. (2014). Converging circuits mediate temperature and shock aversive olfactory conditioning in Drosophila. Curr. Biol. *24*, 1712–1722.

Gorczyca, M.G., and Hall, J.C. (1987). Immunohistochemical localization of choline acetyltransferase during development and in Chats mutants of Drosophila melanogaster. J. Neurosci. *7*, 1361–1369.

Greenspan, R. (1980). Mutations of Choline Acetyltransferase and associated neural defects in *Drosophila melanogaster*. J. Comp. Physiol. *137*, 83–92.

Heisenberg, M. (2003). Mushroom body memoir: from maps to models. Nat. Rev. Neurosci. *4*, 266–275.

Hige, T., Aso, Y., Modi, M.N., Rubin, G.M., and Turner, G.C. (2015). Heterosynaptic Plasticity Underlies Aversive Olfactory Learning in Drosophila. Neuron *88*, 985–998.

Honegger, K.S., Campbell, R.A., and Turner, G.C. (2011). Cellular-resolution population imaging reveals robust sparse coding in the Drosophila mushroom body. J. Neurosci. *31*, 11772–11785.

Huetteroth, W., Perisse, E., Lin, S., Klappenbach, M., Burke, C., and Waddell, S. (2015). Sweet taste and nutrient value subdivide rewarding dopaminergic neurons in Drosophila. Curr. Biol. *25*, 751–758.

Jenett, A., Rubin, G.M., Ngo, T.T., Shepherd, D., Murphy, C., Dionne, H., Pfeiffer, B.D., Cavallaro, A., Hall, D., Jeter, J., et al. (2012). A GAL4-driver line resource for Drosophila neurobiology. Cell Rep. *2*, 991–1001.

Johard, H.A., Enell, L.E., Gustafsson, E., Trifilieff, P., Veenstra, J.A., and Nässel, D.R. (2008). Intrinsic neurons of Drosophila mushroom bodies express short neuropeptide F: relations to extrinsic neurons expressing different neurotransmitters. J. Comp. Neurol. *507*, 1479–1496.

Kandel, E.R., Dudai, Y., and Mayford, M.R. (2014). The molecular and systems biology of memory. Cell *157*, 163–186.

Kim, Y.C., Lee, H.G., and Han, K.A. (2007). D1 dopamine receptor dDA1 is required in the mushroom body neurons for aversive and appetitive learning in Drosophila. J. Neurosci. *27*, 7640–7647.

Kirkhart, C., and Scott, K. (2015). Gustatory learning and processing in the Drosophila mushroom bodies. J. Neurosci. *35*, 5950–5958.

Kitamoto, T., Wang, W., and Salvaterra, P.M. (1998). Structure and organization of the Drosophila cholinergic locus. J. Biol. Chem. *273*, 2706–2713.

Klapoetke, N.C., Murata, Y., Kim, S.S., Pulver, S.R., Birdsey-Benson, A., Cho, Y.K., Morimoto, T.K., Chuong, A.S., Carpenter, E.J., Tian, Z., et al. (2014). Independent optical excitation of distinct neural populations. Nat. Methods *11*, 338–346.

Knapek, S., Kahsai, L., Winther, A.M., Tanimoto, H., and Nässel, D.R. (2013). Short neuropeptide F acts as a functional neuromodulator for olfactory memory in Kenyon cells of Drosophila mushroom bodies. J. Neurosci. *33*, 5340–5345.

Krashes, M.J., DasGupta, S., Vreede, A., White, B., Armstrong, J.D., and Waddell, S. (2009). A neural circuit mechanism integrating motivational state with memory expression in Drosophila. Cell *139*, 416–427.

Lansdell, S.J., Collins, T., Goodchild, J., and Millar, N.S. (2012). The Drosophila nicotinic acetylcholine receptor subunits Dα5 and Dα7 form functional homomeric and heteromeric ion channels. BMC Neurosci. *13*, 73.

Le Novère, N., Corringer, P.J., and Changeux, J.P. (2002). The diversity of subunit composition in nAChRs: evolutionary origins, physiologic and pharmacologic consequences. J. Neurobiol. *53*, 447–456.

Lewis, L.P., Siju, K.P., Aso, Y., Friedrich, A.B., Bulteel, A.J., Rubin, G.M., and Grunwald Kadow, I.C. (2015). A Higher Brain Circuit for Immediate Integration of Conflicting Sensory Information in Drosophila. Curr. Biol. *25*, 2203–2214.

Lin, A.C., Bygrave, A.M., de Calignon, A., Lee, T., and Miesenböck, G. (2014a). Sparse, decorrelated odor coding in the mushroom body enhances learned odor discrimination. Nat. Neurosci. *17*, 559–568.

Lin, S., Owald, D., Chandra, V., Talbot, C., Huetteroth, W., and Waddell, S. (2014b). Neural correlates of water reward in thirsty Drosophila. Nat. Neurosci. *17*, 1536–1542.

Liu, C., Plaçais, P.Y., Yamagata, N., Pfeiffer, B.D., Aso, Y., Friedrich, A.B., Siwanowicz, I., Rubin, G.M., Preat, T., and Tanimoto, H. (2012). A subset of dopamine neurons signals reward for odour memory in Drosophila. Nature *488*, 512–516.

Mao, Z., and Davis, R.L. (2009). Eight different types of dopaminergic neurons innervate the Drosophila mushroom body neuropil: anatomical and physiological heterogeneity. Front. Neural Circuits *3*, 5.

Mauss, A.S., Meier, M., Serbe, E., and Borst, A. (2014). Optogenetic and pharmacologic dissection of feedforward inhibition in Drosophila motion vision. J. Neurosci. *34*, 2254–2263.

McGuire, S.E., Le, P.T., Osborn, A.J., Matsumoto, K., and Davis, R.L. (2003). Spatiotemporal rescue of memory dysfunction in Drosophila. Science *302*, 1765–1768.

Menzel, R. (2014). The insect mushroom body, an experience-dependent recoding device. J. Physiol. Paris *108*, 84–95.

Murthy, M., Fiete, I., and Laurent, G. (2008). Testing odor response stereotypy in the Drosophila mushroom body. Neuron *59*, 1009–1023.

Ni, J.Q., Liu, L.P., Binari, R., Hardy, R., Shim, H.S., Cavallaro, A., Booker, M., Pfeiffer, B.D., Markstein, M., Wang, H., et al. (2009). A Drosophila resource of transgenic RNAi lines for neurogenetics. Genetics *182*, 1089–1100.

Owald, D., and Waddell, S. (2015). Olfactory learning skews mushroom body output pathways to steer behavioral choice in Drosophila. Curr. Opin. Neurobiol. *35*, 178–184.

Owald, D., Felsenberg, J., Talbot, C.B., Das, G., Perisse, E., Huetteroth, W., and Waddell, S. (2015). Activity of defined mushroom body output neurons underlies learned olfactory behavior in Drosophila. Neuron *86*, 417–427.

Pai, T.P., Chen, C.C., Lin, H.H., Chin, A.L., Lai, J.S., Lee, P.T., Tully, T., and Chiang, A.S. (2013). Drosophila ORB protein in two mushroom body output neurons is necessary for long-term memory formation. Proc. Natl. Acad. Sci. USA *110*, 7898–7903.

Perisse, E., Burke, C., Huetteroth, W., and Waddell, S. (2013a). Shocking revelations and saccharin sweetness in the study of Drosophila olfactory memory. Curr. Biol. *23*, R752–R763.

Perisse, E., Yin, Y., Lin, A.C., Lin, S., Huetteroth, W., and Waddell, S. (2013b). Different kenyon cell populations drive learned approach and avoidance in Drosophila. Neuron *79*, 945–956.

Perrat, P.N., DasGupta, S., Wang, J., Theurkauf, W., Weng, Z., Rosbash, M., and Waddell, S. (2013). Transposition-driven genomic heterogeneity in the Drosophila brain. Science *340*, 91–95.

Pitman, J.L., Huetteroth, W., Burke, C.J., Krashes, M.J., Lai, S.L., Lee, T., and Waddell, S. (2011). A pair of inhibitory neurons are required to sustain labile memory in the Drosophila mushroom body. Curr. Biol. *21*, 855–861.

Plaçais, P.Y., Trannoy, S., Friedrich, A.B., Tanimoto, H., and Preat, T. (2013). Two pairs of mushroom body efferent neurons are required for appetitive long-term memory retrieval in Drosophila. Cell Rep. *5*, 769–780.

Pologruto, T.A., Sabatini, B.L., and Svoboda, K. (2003). ScanImage: flexible software for operating laser scanning microscopes. Biomed. Eng. Online *2*, 13.

Qin, H., Cressy, M., Li, W., Coravos, J.S., Izzi, S.A., and Dubnau, J. (2012). Gamma neurons mediate dopaminergic input during aversive olfactory memory formation in Drosophila. Curr. Biol. *22*, 608–614.

Roberts, A.C., and Glanzman, D.L. (2003). Learning in Aplysia: looking at synaptic plasticity from both sides. Trends Neurosci. *26*, 662–670.

Root, C.M., Ko, K.I., Jafari, A., and Wang, J.W. (2011). Presynaptic facilitation by neuropeptide signaling mediates odor-driven food search. Cell *145*, 133–144.

Salin, P.A., Malenka, R.C., and Nicoll, R.A. (1996). Cyclic AMP mediates a presynaptic form of LTP at cerebellar parallel fiber synapses. Neuron *16*, 797–803.

Schäfer, S., Bicker, G., Ottersen, O.P., and Storm-Mathisen, J. (1988). Taurine-like immunoreactivity in the brain of the honeybee. J. Comp. Neurol. *268*, 60–70.

Schürmann, F.W. (2000). Acetylcholine, GABA, glutamate and NO as putative transmitters indicated by immunocytochemistry in the olfactory mushroom body system of the insect brain. Acta Biol. Hung. *51*, 355–362.

Séjourné, J., Plaçais, P.Y., Aso, Y., Siwanowicz, I., Trannoy, S., Thoma, V., Tedjakumala, S.R., Rubin, G.M., Tchénio, P., Ito, K., et al. (2011). Mushroom body efferent neurons responsible for aversive olfactory memory retrieval in Drosophila. Nat. Neurosci. *14*, 903–910.

Shang, Y., Claridge-Chang, A., Sjulson, L., Pypaert, M., and Miesenböck, G. (2007). Excitatory local circuits and their implications for olfactory processing in the fly antennal lobe. Cell *128*, 601–612.

Shih, H.W., Wu, C.L., Chang, S.W., Liu, T.H., Lai, J.S., Fu, T.F., Fu, C.C., and Chiang, A.S. (2015). Parallel circuits control temperature preference in Drosophila during ageing. Nat. Commun. *6*, 7775.

Shomrat, T., Graindorge, N., Bellanger, C., Fiorito, G., Loewenstein, Y., and Hochner, B. (2011). Alternative sites of synaptic plasticity in two homologous "fan-out fan-in" learning and memory networks. Curr. Biol. *21*, 1773–1782.

Sinakevitch, I., Farris, S.M., and Strausfeld, N.J. (2001). Taurine-, aspartate- and glutamate-like immunoreactivity identifies chemically distinct subdivisions of Kenyon cells in the cockroach mushroom body. J. Comp. Neurol. *439*, 352–367.

Sitaraman, D., Aso, Y., Jin, X., Chen, N., Felix, M., Rubin, G.M., and Nitabach, M.N. (2015). Propagation of Homeostatic Sleep Signals by Segregated Synaptic Microcircuits of the Drosophila Mushroom Body. Curr. Biol. *25*, 2915–2927.

Stevens, C.F. (2015). What the fly's nose tells the fly's brain. Proc. Natl. Acad. Sci. USA *112*, 9460–9465.

Strausfeld, N.J., Hansen, L., Li, Y., Gomez, R.S., and Ito, K. (1998). Evolution, discovery, and interpretations of arthropod mushroom bodies. Learn. Mem. *5*, 11–37.

Strausfeld, N.J., Sinakevitch, I., and Vilinsky, I. (2003). The mushroom bodies of Drosophila melanogaster: an immunocytological and golgi study of Kenyon cell organization in the calyces and lobes. Microsc. Res. Tech. *62*, 151–169.

Strausfeld, N.J., Sinakevitch, I., Brown, S.M., and Farris, S.M. (2009). Ground plan of the insect mushroom body: functional and evolutionary implications. J. Comp. Neurol. *513*, 265–291.

Tanaka, N.K., Tanimoto, H., and Ito, K. (2008). Neuronal assemblies of the Drosophila mushroom body. J. Comp. Neurol. *508*, 711–755.

Thany, S.H., Lenaers, G., Raymond-Delpech, V., Sattelle, D.B., and Lapied, B. (2007). Exploring the pharmacological properties of insect nicotinic acetylcholine receptors. Trends Pharmacol. Sci. *28*, 14–22.

Tomer, R., Denes, A.S., Tessmar-Raible, K., and Arendt, D. (2010). Profiling by image registration reveals common origin of annelid mushroom bodies and vertebrate pallium. Cell *142*, 800–809.

Trannoy, S., Redt-Clouet, C., Dura, J.M., and Preat, T. (2011). Parallel processing of appetitive short- and long-term memories in Drosophila. Curr. Biol. *21*, 1647–1653.

Tully, T., and Quinn, W.G. (1985). Classical conditioning and retention in normal and mutant Drosophila melanogaster. J. Comp. Physiol. A Neuroethol. Sens. Neural Behav. Physiol. *157*, 263–277.

Vecsey, C.G., Pírez, N., and Griffith, L.C. (2014). The Drosophila neuropeptides PDF and sNPF have opposing electrophysiological and molecular effects on central neurons. J. Neurophysiol. *111*, 1033–1045.

Vogt, K., Schnaitmann, C., Dylla, K.V., Knapek, S., Aso, Y., Rubin, G.M., and Tanimoto, H. (2014). Shared mushroom body circuits underlie visual and olfactory memories in Drosophila. eLife *3*, e02395.

Waddell, S. (2013). Reinforcement signalling in Drosophila; dopamine does it all after all. Curr. Opin. Neurobiol. *23*, 324–329.

Wagh, D.A., Rasse, T.M., Asan, E., Hofbauer, A., Schwenkert, I., Dürrbeck, H., Buchner, S., Dabauvalle, M.C., Schmidt, M., Qin, G., et al. (2006). Bruchpilot, a protein with homology to ELKS/CAST, is required for structural integrity and function of synaptic active zones in Drosophila. Neuron *49*, 833–844.

Wang, J.W., Wong, A.M., Flores, J., Vosshall, L.B., and Axel, R. (2003). Two-photon calcium imaging reveals an odor-evoked map of activity in the fly brain. Cell *112*, 271–282.

Wu, J.S., and Luo, L. (2006). A protocol for dissecting Drosophila melanogaster brains for live imaging or immunostaining. Nat. Protoc. *1*, 2110–2115.

Yamagata, N., Ichinose, T., Aso, Y., Plaçais, P.Y., Friedrich, A.B., Sima, R.J., Preat, T., Rubin, G.M., and Tanimoto, H. (2015). Distinct dopamine neurons mediate reward signals for short- and long-term memories. Proc. Natl. Acad. Sci. USA *112*, 578–583.

Yasuyama, K., Kitamoto, T., and Salvaterra, P.M. (1995a). Localization of choline acetyltransferase-expressing neurons in the larval visual system of Drosophila melanogaster. Cell Tissue Res. *282*, 193–202.

Yasuyama, K., Kitamoto, T., and Salvaterra, P.M. (1995b). Immunocytochemical study of choline acetyltransferase in Drosophila melanogaster: an analysis of cis-regulatory regions controlling expression in the brain of cDNA-transformed flies. J. Comp. Neurol. *361*, 25–37.

Yasuyama, K., Meinertzhagen, I.A., and Schürmann, F.W. (2002). Synaptic organization of the mushroom body calyx in Drosophila melanogaster. J. Comp. Neurol. *445*, 211–226.

Zars, T., Fischer, M., Schulz, R., and Heisenberg, M. (2000). Localization of a short-term memory in Drosophila. Science *288*, 672–675.